Finite-difference lattice Boltzmann model with flux limiters for liquid-vapor systems

V. Sofonea,[1,2,*] A. Lamura,[3,†] G. Gonnella,[1,4,‡] and A. Cristea[2,§]
[1]*Dipartimento di Fisica, Università di Bari, Via Amendola 173, 70126 Bari, Italy*
[2]*Laboratory for Numerical Simulation and Parallel Computing in Fluid Mechanics, Center for Fundamental and Advanced Technical Research, Romanian Academy, Boulevard Mihai Viteazul 24, 300223 Timişoara, Romania*
[3]*Istituto Applicazioni Calcolo, CNR, Sezione di Bari, Via Amendola 122/D, 70126 Bari, Italy*
[4]*TIRES, Center of Innovative Technologies for Signal Detection and Processing, and INFM, Unità di Bari, and INFN, Sezione di Bari, Via Amendola 173, 70126 Bari, Italy*
(Received 26 March 2004; published 6 October 2004)

In this paper we apply a finite difference lattice Boltzmann model to study the phase separation in a two-dimensional liquid-vapor system. Spurious numerical effects in macroscopic equations are discussed and an appropriate numerical scheme involving flux limiter techniques is proposed to minimize them and guarantee a better numerical stability at very low viscosity. The phase separation kinetics is investigated and we find evidence of two different growth regimes depending on the value of the fluid viscosity as well as on the liquid-vapor ratio.

DOI: 10.1103/PhysRevE.70.046702 PACS number(s): 47.11.+j, 47.20.Hw, 05.70.Ln

I. INTRODUCTION

Lattice Boltzmann (LB) models approach physical phenomena in fluid systems using a phase-space discretized form of the Boltzmann equation [1–5]. Conservation equations are derived by calculating moments of various order of this equation [6–12]. After the publication of the first LB model which exhibits phase separation [13,14], LB models were widely used to investigate the complex behavior of single- or multicomponent/phase fluid systems [3,5] and refer mainly to isothermal systems [15–25]. This limitation comes from the constant value of the lattice speed c_l which in LB models is related to the temperature T, the lattice spacing δs and the time step δt through two separate relations

$$c_l = \frac{c_s}{\sqrt{\chi}} = \sqrt{\frac{k_B T}{\chi m}}, \tag{1}$$

$$c_l = \frac{\delta s}{\delta t}, \tag{2}$$

where $c_s = \sqrt{k_B T/m}$ is the isothermal speed of sound for an ideal fluid, m is the mass of fluid particles, χ is a constant depending on the geometry of the lattice, and k_B is Boltzmann's constant [5,26].

According to the "collide and stream" philosophy of LB models, fluid collides in the lattice nodes and thereafter moves along the lattice links in a lapse δt towards neighboring nodes with the speed c_l given by Eq. (2) [2–5]. Such a relationship is no longer considered in finite difference lattice Boltzmann (FDLB) models [27–31] which start directly from the Boltzmann equation and have a better numerical stability. In such models there is more freedom to choose the discrete velocity set, as done recently in the thermal FDLB model of Watari and Tsutahara [32] where the possibility of having different sets of velocities allows to release the constraint of constant temperature. Also, the use of FDLB models is promising, e.g., when considering LB models for multicomponent fluid systems, where the masses of the components are not identical and Eq. (1) would lead to different lattice speeds. In this context, FDLB models may be viewed as a convenient alternative to interpolation supplemented LB models [33–35].

FDLB models, as well as LB models, are known to introduce spurious terms in the mass and momentum conservation equations, which are dependent on the lattice spacing δs and the time step δt [31]. The behavior of an isothermal fluid system subjected to FDLB simulation is governed by the apparent values of the viscosity and/or diffusivity. The expression of these quantities with respect to δs and δt depends on the finite difference scheme used in the FDLB model. Consequently, the choice of the numerical scheme may alter significantly the macroscopic behavior of the fluid system observed during simulations as well as the numerical stability. This problem still lacks necessary clarification and should be always considered in order to recover the correct physical interpretation of simulation results.

The purpose of this paper is to investigate these numerical aspects by using a FDLB model addressing the phase separation kinetics in a van der Waals fluid. Phase separation in liquid-vapor systems has not received as much attention as in binary fluids [36]. Under the hypothesis of dynamical scaling the late time kinetics can be characterized in terms of a single length scale $R(t)$ which grows according to the power law $R(t) \sim t^{\alpha}$, where α is the growth exponent [37]. The late time growth, when hydrodynamics is neglected, is expected to be described by the Allen-Cahn theory which gives a growth exponent $\alpha = 1/2$ [38]. When hydrodynamics comes

*Electronic address: sofonea@acad-tim.tm.edu.ro
†Electronic address: a.lamura@area.ba.cnr.it; http://www.ba.cnr.it/~irmaal21
‡Electronic address: gonnella@ba.infn.it
§Permanent address of V. Sofonea. Electronic address: flastra@acad-tim.tm.edu.ro

into play, the liquid-vapor system behaves similarly to binary fluids so that a growth exponent $\alpha=2/3$ is expected [36]. Previous numerical studies used molecular dynamics simulations [39,40] and a LB model based on a free energy functional [41–43]. In molecular dynamics simulations it was found evidence for the growth exponent $1/2$ [39,40]. By using the free-energy LB model, Osborn *et al.* [41] found the growth exponents $2/3$ and $1/2$ at low and high viscosity, respectively, independently on the system composition. Mecke and Sofonea [42,43], using the same algorithm for an off-symmetric system, found a crossover from $2/3$ to $1/2$ at low viscosity, and $1/3$ at high viscosity. We will compare results of our model with the aforementioned ones.

To model the liquid-vapor system, a standard force term [13,14,25] is added to the discretized Boltzmann equations. The resulting FDLB model is described in Sec. II. In Sec. III we introduce two numerical schemes, namely, the first order upwind finite difference scheme and a higher order one which uses flux limiters [44,45]. There we show the difference between FDLB, collide and stream LB and volumetric LB models [46,47]. We thereafter discuss the spurious numerical effects these schemes introduce in the fluid equations. Section IV reports the simulation results, where special attention was given to the effects of the numerical schemes on estimation of the growth exponent. In order to clarify the phenomenology and estimate accurately the exponent α, we monitored the size of domains $R(t)$ by using three independent measures. A discussion about the method and results ends the paper.

II. THE MODEL

The two-dimensional (2D) FDLB model follows the LB model for nonideal fluids [13,14,21,48,49]. The starting point is provided by the set of $\mathcal{N}$ partial derivatives equations resulting from the discretization of the Boltzmann equation on a square lattice $\mathcal{L}$ when the collision term is linearized using the BGK approximation [50]. In nondimensional form, this set reads

$$\partial_t f_i + e_{i\beta}\partial_\beta f_i = \frac{1}{\chi c^2} f_i^{\mathrm{eq}}(e_{i\beta}-u_\beta)F_\beta - \frac{1}{\tau}(f_i - f_i^{\mathrm{eq}}),$$

$$i = 0,1,\ldots\mathcal{N}. \tag{3}$$

Since we will deal with a van der Waals fluid, we used the following reference quantities for particle number density, temperature and speed to get the nondimensional form (3) of the discretized Boltzmann equations: $n_R=N_A/V_{\mathrm{mc}}$, $T_R=T_c$, $c_R=\sqrt{k_B T_c/m}$. Here N_A is Avogadro's number, V_{mc} is the molar volume at the critical point, and T_c is the critical temperature. With this choice of reference quantities, the dimensionless speed is [51]:

$$c = c_l/c_R = \sqrt{\theta/\chi}, \tag{4}$$

where $\theta=T/T_R$ is the dimensionless temperature and the constant χ equals $1/3$ for the square lattice we use (see later for details on the lattice) [31]. If we take the system size as the reference length l_R, we get the reference time t_R from the condition $t_R c_R = l_R$. The nondimensionalized lattice spacing is defined by the number of lattice nodes N we choose along the nondimensionalized system length L:

$$\delta s = \frac{L}{N}. \tag{5}$$

The particle distribution functions $f_i \equiv f_i(\boldsymbol{x},t)$ are defined in the nodes $\boldsymbol{x}$ of the square lattice $\mathcal{L}$. In the $D2Q9$ (2 dimensions, 9 velocities) model we use in this paper, $\mathcal{N}=8$ and the velocities $\boldsymbol{e}_i$ are [2–5]:

$$\boldsymbol{e}_0 = \boldsymbol{0},$$

$$\boldsymbol{e}_i = \left(\cos\frac{\pi(i-1)}{2},\ \sin\frac{\pi(i-1)}{2}\right)c \quad (i=1,\ldots,4),$$

$$\boldsymbol{e}_i = \left(\cos\left(\frac{\pi}{4}+\frac{\pi(i-5)}{2}\right),\ \sin\left(\frac{\pi}{4}+\frac{\pi(i-5)}{2}\right)\right)c\sqrt{2} \quad (i=5,\ldots,8). \tag{6}$$

The equilibrium distribution functions $f_i^{\mathrm{eq}}=f_i^{\mathrm{eq}}(\boldsymbol{x},t)$ are expressed as series expansions of the Maxwellian distribution function, up to second order with respect to the local velocity $\boldsymbol{u}=\boldsymbol{u}(\boldsymbol{x},t)$, whose Cartesian components are u_β [52]:

$$f_i^{\mathrm{eq}} = w_i n\left[1 + \frac{\boldsymbol{e}_i\cdot\boldsymbol{u}}{\chi c^2} + \frac{(\boldsymbol{e}_i\cdot\boldsymbol{u})^2}{2\chi^2 c^4} - \frac{(\boldsymbol{u})^2}{2\chi c^2}\right]. \tag{7}$$

The weight coefficients are

$$w_i = \begin{cases} \frac{4}{9} & (i=0) \\ \frac{1}{9} & (i=1,\ldots,4) \\ \frac{1}{36} & (i=5,\ldots,8). \end{cases} \tag{8}$$

The local density $n=n(\boldsymbol{x},t)$, as well as the components of the local velocity $\boldsymbol{u}$ which enter Eq. (7), are calculated from the distribution functions as follows:

$$n = \sum_i f_i = \sum_i f_i^{\mathrm{eq}}, \tag{9}$$

$$u_\beta = \frac{1}{n}\sum_i f_i e_{i\beta} = \frac{1}{n}\sum_i f_i^{\mathrm{eq}} e_{i\beta}. \tag{10}$$

The force term in Eqs. (3) is given by [48,49]:

$$F_\beta = \frac{1}{n}\partial_\beta(p^i - p^w) + \kappa\partial_\beta(\nabla^2 n), \tag{11}$$

where

$$p^i = \theta n \tag{12}$$

and

$$p^w = \frac{3\theta n}{3-n} - \tfrac{9}{8}n^2 \tag{13}$$

are the nondimensionalized pressures of the ideal and the van der Waals fluid, respectively [51]. With the equation of state

in the form (13), the critical point is located at $\theta=1$ and $n=1$. The parameter κ controls the surface tension [25]. The mass and momentum equations are recovered from Eqs. (3) after using the standard Chapman-Enskog procedure up to second order with respect to Knudsen number $\mathrm{Kn}=c\tau/L$. These equations read [4,5,25]:

$$\partial_t n + \partial_\beta(nu_\beta) = 0, \tag{14}$$

$$\partial_t(nu_\alpha) + \partial_\beta(nu_\alpha u_\beta) = -\partial_\alpha p^w + \kappa n\partial_\alpha(\nabla^2 n) + \nu\partial_\beta[n(\partial_\alpha u_\beta + \partial_\beta u_\alpha)], \tag{15}$$

where

$$\nu = \chi c^2 \tau \tag{16}$$

is the *physical value* of the kinematic viscosity [31]. The particular numerical scheme used to solve Eqs. (3) may introduce a spurious viscosity term that adds to the physical value, as seen in the next section. Finally, we note that the force term (11) allows to recover the Navier-Stokes equation (15) where the pressure p^w appearing on the right-hand side is subjected to the van der Waals equation of state (13).

III. FINITE DIFFERENCE SCHEMES

A. First-order upwind scheme

The set of phase space discretized equations (3) may be solved numerically by using an appropriate finite difference scheme defined on the lattice $\mathcal{L}$. Simple second-order schemes like the centered one or the Lax-Wendroff scheme [44,45,53] are unstable because of large values of the density gradient which may occur in the interface regions separating the liquid and vapor phases of the van der Waals fluid. The first-order upwind scheme, which is also used in LB models [2–5], is a good candidate because of its stability. When associated to the forward time stepping rule, this scheme gives the following updating rule for the distribution functions defined in node $\boldsymbol{x}\in\mathcal{L}$ [31]:

$$f_i(\boldsymbol{x},t+\delta t) = f_i(\boldsymbol{x},t) - \frac{c\delta t}{\delta s}[f_i(\boldsymbol{x},t) - f_i(\boldsymbol{x}-\delta s\boldsymbol{e}_i/c,t)] + \delta t Q_i(\boldsymbol{x},t), \tag{17,18}$$

where

$$Q_i = Q_i(\boldsymbol{x},t) = \frac{1}{\theta}\left\{\frac{1}{n(\boldsymbol{x},t)}\partial_\beta[p^i(\boldsymbol{x},t) - p^w(\boldsymbol{x},t)] + \kappa\partial_\beta[\nabla^2 n(\boldsymbol{x},t)]\right\} \times f_i^{\mathrm{eq}}(\boldsymbol{x},t)[e_{i\beta} - u_\beta(\boldsymbol{x},t)] - \frac{1}{\tau}[f_i(\boldsymbol{x},t) - f_i^{\mathrm{eq}}(\boldsymbol{x},t)], \tag{19}$$

$$i = 0,1,\ldots,\mathcal{N}.$$

As discussed in Ref. [31], finite difference schemes introduce spurious numerical terms in the conservation equations. This happens because the *real* evolution equations recovered (up to second order in space and time) from the updating rules (17) are

$$\partial_t f_i + \phi\partial_t^2 f_i + e_{i\beta}\partial_\beta f_i - \psi\partial_\beta\partial_\gamma e_{i\beta}e_{i\gamma}f_i = Q_i, \quad i = 0,1,\ldots,\mathcal{N}, \tag{20}$$

where

$$\phi = \frac{\delta t}{2}, \tag{21}$$

$$\psi = \frac{\delta s}{2c}. \tag{22}$$

We get the following form of the conservation equations up to second order in the Knudsen number:

$$\partial_t n + \partial_\beta(nu_\beta) = (\psi-\phi)\partial_\alpha\partial_\beta(\chi c^2 n\delta_{\alpha\beta} + nu_\alpha u_\beta), \tag{23}$$

$$\partial_t(nu_\alpha) + \partial_\beta(nu_\alpha u_\beta) = -\partial_\alpha p^w + \kappa n\partial_\alpha(\nabla^2 n) + \nu_{\mathrm{ap}}\partial_\beta[n(\partial_\alpha u_\beta + \partial_\beta u_\alpha)] + \chi c^2(\psi-\phi)\partial_\beta[\partial_\alpha(nu_\beta) + u_\beta\partial_\alpha n + u_\alpha\partial_\beta n]. \tag{24}$$

Thus, the finite difference scheme introduces spurious terms, depending on the quantity $(\psi-\phi)$, in both the conservation equations [compare with Eqs. (14)–(15)], while the physical value (16) of the kinematic viscosity is replaced by the *apparent value* [31]:

$$\nu_{\mathrm{ap}} = \chi c^2(\tau+\psi). \tag{25}$$

One could use δs, δt, and c such that $\psi=\phi\Leftrightarrow\delta s=c\delta t$ and remove spurious terms in the Eqs. (23)–(24). In this case it would be $\nu_{\mathrm{ap}}=\chi c^2(\tau+\delta t/2)$. In order to maintain the apparent value of the viscosity close to the physical one and allow very small values of ν, one should require $\delta t\ll\tau$. Since the condition $\psi=\phi$ is equivalent to ask $N=L/c\delta t$, one should have $N\gtrsim 10^4$ when $\tau\lesssim 10^{-3}$, being $c\simeq L\simeq 1$. This would require a huge computational effort when doing 2D or three-dimensional simulations using the first order upwind FDLB model. Higher order flux limiter schemes provide a possibility to overcome this problem giving a better stability. As we will see further, these schemes improve the accuracy of the FDLB simulations with respect to the upwind scheme, for the same value of the number N of lattice nodes.

As a matter of comparison we recall that the collide and stream LB model is equivalent to an upwind FDLB model, when also the relaxation term is calculated on the characteristics line [31] and the choice $\delta s=c\delta t$ is adopted. The resulting apparent value of the viscosity is $\nu_{\mathrm{ap}}=\chi c^2(\tau-\delta t/2)$. For this reason the collide and stream LB model suffers mainly from the lack of stability when $\tau\simeq\delta t/2$ so that very low values of viscosity cannot be accessed [25].

B. Flux limiter schemes

Figure 1 shows two characteristics lines on the square lattice involving the distribution functions $f_1(\boldsymbol{x},t)$ and $f_5(\boldsymbol{x},t)$, respectively. For convenience, we denote $g_{i,j}^k$ the value of the quantity g_i in node j at time $t=k\delta t$. According to the general procedure to construct high order total variation diminishing schemes using flux limiters [44,45,53] we re-

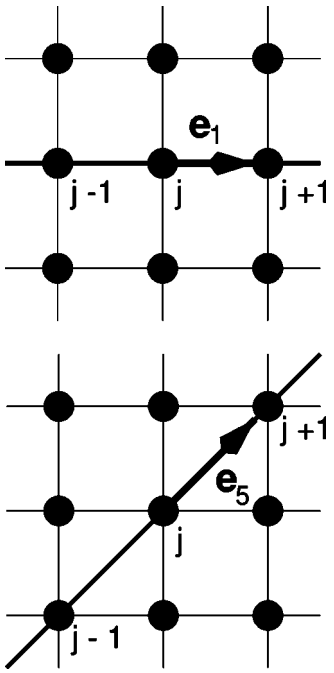

FIG. 1. Characteristics lines on the square lattice, for the directions e_1 (a) and e_5 (b).

write the updating rule (17) in a conservative form using two fluxes [54–56]:

$$f_{i,j}^{k+1} = f_{i,j}^{k} - \frac{c\,\delta t}{\delta s}(F_{i,j+1/2}^{k} - F_{i,j-1/2}^{k}) + \delta t Q_{i,j}^{k}, \tag{26}$$

where

$$F_{i,j+1/2}^{k} = f_{i,j}^{k} + \frac{1}{2}\left(1 - \frac{c\,\delta t}{\delta s}\right)(f_{i,j+1}^{k} - f_{i,j}^{k})\Psi(\Theta_{i,j}^{k}) \tag{27}$$

and

$$F_{i,j-1/2}^{n} = F_{i,(j-1)+1/2}^{n}. \tag{28}$$

The flux limiter $\Psi(\Theta_{i,j}^{n})$ introduced in Eq. (27) is expressed as a function of the *smoothness*

$$\Theta_{i,j}^{n} = \frac{f_{i,j}^{n} - f_{i,j-1}^{n}}{f_{i,j+1}^{n} - f_{i,j}^{n}}. \tag{29}$$

In particular, the second order Lax-Wendroff scheme is recovered for $\Psi(\Theta_{i,j}^{n})=1$. The upwind scheme, described in the previous subsection, is recovered as another particular case, when $\Psi(\Theta_{i,j}^{n})=0$. A wide choice of flux limiters are at our disposal in the literature [44,45,53]. LB simulations reported in this paper were done using the monitorized central difference limiter [44]:

$$\Psi(\Theta_{i,j}^{n}) = \begin{cases} 0 & , \quad \Theta_{i,j}^{n} \leqslant 0 \\ 2\Theta_{i,j}^{n} & , \quad 0 \leqslant \Theta_{i,j}^{n} \leqslant \frac{1}{3} \\ \dfrac{1+\Theta_{i,j}^{n}}{2} & , \quad \frac{1}{3} \leqslant \Theta_{i,j}^{n} \leqslant 3 \\ 2 & , \quad 3 \leqslant \Theta_{i,j}^{n} \end{cases} \tag{30}$$

but other limiters give qualitatively similar results.

Equations (26) satisfy the global particle and momentum conservation. When using the first order upwind scheme, the spurious terms introduced in the mass and momentum conservation equations are linearly dependent on the lattice spacing δs. Since flux limiter schemes are adapting themselves to the local smoothness (29) of the distribution functions, it is rather cumbersome to derive analytical expressions of the spurious numerical term ψ in these cases. LB simulations of diffusion phenomena done using flux limiter schemes suggest a second order dependence of the value ψ on the lattice spacing δs [57] such that $\psi=(\delta s)^2/2cL$ and the apparent value of the kinematic viscosity (25) becomes

$$\nu_{\text{ap\_flux}} = \chi c^2\left[\tau + \frac{(\delta s)^2}{2cL}\right]. \tag{31}$$

When the lattice spacing is a small quantity, the use of flux limiter schemes is expected to improve the accuracy of FDLB simulations as well as the stability.

A different approach that allows to avoid spurious terms in the conservation equations is provided by the volumetric LB scheme introduced in Ref. [46] which satisfies detailed balance and achieves the desired order of accuracy. We will refer to the fractional version of the aforementioned scheme constructed in the case of a homogeneous fluid on a uniform mesh [47] since we are using a regular and uniform lattice. In the scheme proposed in Ref. [47] the value of the viscosity can be reduced with respect to the collide and stream LB and the Courant-Friedrichs-Levy number $\text{CFL}=c\,\delta t/\delta s$ can be smaller than 1. Moreover, some unphysical spurious invariants are removed. Our scheme can have very small values of viscosity since the numerical contribution to the value of viscosity, proportional to ψ, can be reduced and made much smaller than the physical term, proportional to τ, without having stability problems. This depends on the fact the in finite difference schemes the values of δs and δt can be set independently from the value of c. Our choice of δt and δs is such to guarantee that the CFL number is much less than 1 and that the unavoidable spurious terms, introduced by the numerical scheme and proportional to $(\psi-\phi)$, can be done as small as desired.

IV. SIMULATION RESULTS

In this section we report the results of our simulations. For all runs we used $N=1024$, $\delta s=1/256$, and $\delta t=10^{-5}$. In the following, lengths are expressed in units of lattice spacing and time is expressed as the product of algorithm steps by δt. All quenches below the critical temperature were to the temperature $\theta=0.79$ where the coexisting densities are $n_{\text{liquid}}=1.956$ and $n_{\text{vapor}}=0.226$. Each simulation was started

with small fluctuations (0.1%) in the density about a mean value $\hat{n}$ that was either symmetric ($\hat{n}=1.09$, liquid fraction $\beta=0.5$) or slightly off-symmetric ($\hat{n}=1.0, \beta=0.45$). The parameter κ controlling the surface tension was set to 5×10^{-6} to have an interface thickness of ~ 6 lattice spacings. The viscosity was varied by changing τ. We fixed an upper bound of τ by the following argument. It is well known that the continuum hypothesis and the Navier-Stokes equation are valid only for small values of the Knudsen number Kn [58]. Since $\mathrm{Kn}=c\tau/L$ and $c\simeq L\simeq 1$ in our simulations, this means $\tau \lesssim 10^{-2}$. We implemented the upwind and the flux limiter schemes and compared results when $\tau=10^{-4}$. In this case the spurious numerical contribution of the upwind scheme is larger than the physical one. Numerical contributions get negligible when the flux limiter scheme is considered instead. Therefore one expects to observe qualitative and quantitative differences. We used also the value $\tau=10^{-3}$ with the flux limiter scheme to access a higher viscosity regime.

In order to have different and independent tools to estimate the domains size we used the following quantities: $R_1(t)$, the inverse of the length of the interfaces of domains, measured by counting lattice points where the order parameter $\rho(\boldsymbol{x},t)=n(\boldsymbol{x},t)-\hat{n}$ is such that $\rho(\boldsymbol{x},t)\rho(\boldsymbol{x}',t)<0; R_2(t)$, the inverse of the first moment of the spherically averaged structure factor

$$R_2(t)=\pi\frac{\int C(k,t)dk}{\int kC(k,t)dk}, \tag{32}$$

where $k=|\boldsymbol{k}|$ is the modulus of the wave vector in Fourier space, and

$$C(k,t)=<\tilde{\rho}(\boldsymbol{k},t)\tilde{\rho}(-\boldsymbol{k},t)> \tag{33}$$

with $\tilde{\rho}(\boldsymbol{k},t)$ the spatial Fourier transform of the order parameter $\rho(\boldsymbol{x},t)$. The angle brackets denote an average over a shell in $\boldsymbol{k}$ space at fixed k. The last quantity $R_3(t)$ is defined as the inverse of the first moment of the spherically averaged structure factor of the fluid velocity

$$R_3(t)=\pi\frac{\int C_u(k,t)dk}{\int kC_u(k,t)dk} \tag{34}$$

with $C_u(k,t)=<|\tilde{\boldsymbol{u}}(\boldsymbol{k})|^2>$. In all the figures R_1 was multiplied by 4 000 000 to be shown in the same plot with R_2 and R_3.

In Fig. 2 we present the three measures of domains size as function of time for the case $\tau=10^{-4}$ with flux limiter scheme, and symmetric composition. It is interesting to note that R_2 and R_3 have the same trend, with a similar prefactor. This feature holds for all the runs we considered. This last point is not obvious *a priori*. After a swift initial growth the evolution of all quantities suggests the existence of the growth exponent 2/3. This is in accordance with previous studies on symmetric liquid-vapor systems at low viscosity [41] when hydrodynamic flow is operating. In this regime hydrodynamics is the mechanism to get domains circular since the flow is driven by the difference in Laplace pressure between points of different curvature on the boundary of domains. This remark is confirmed when looking at configurations of the density n. In Fig. 3 we show contour plots of a part of the whole system at consecutive times. The vapor bubble in the down left corner at $t=12$, while evaporating, is rounded by the flow as it can be seen by comparing it with the shape at $t=15$.

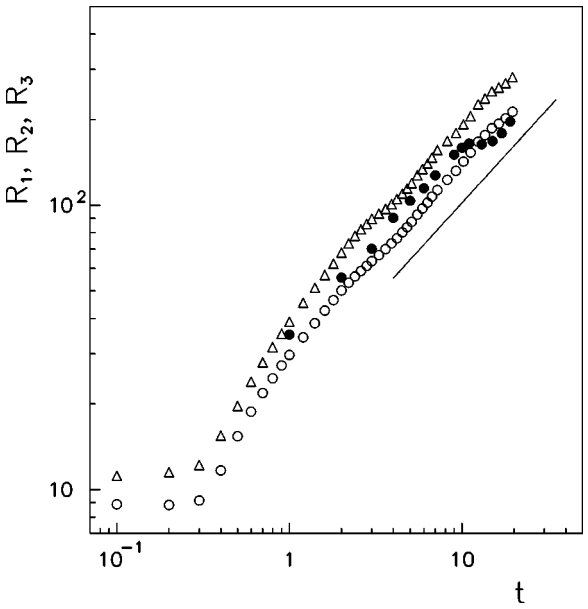

FIG. 2. Evolution of domains size recovered for $\tau=10^{-4}, \beta=0.5$, and the flux limiter scheme: $R_1(\Delta)$, $R_2(\circ)$, $R_3(\bullet)$. R's are measured in lattice spacings and R_1 has been multiplied by 4 000 000 to be shown in the same plot. The straight line has slope 2/3.

An indication about the velocity field comes from the structure factor $C_u(k,t)$. In Fig. 4 we plot it at time $t=15$. It exhibits a structure at a scale comparable with system size. All velocity components decay becoming small at low wave-

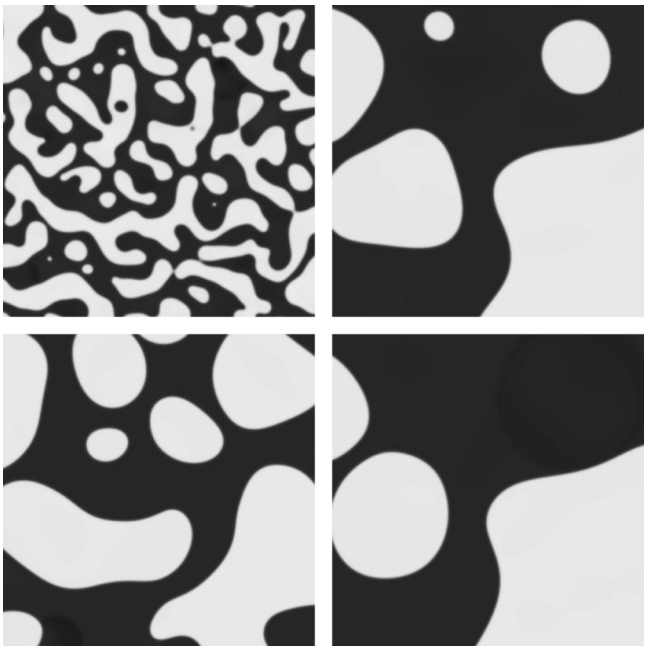

FIG. 3. Contour plots of a portion 512×512 of the whole lattice of the density n in the case with $\tau=10^{-4}, \beta=0.5$, and flux limiter scheme. Color code: black/white → liquid/vapor.

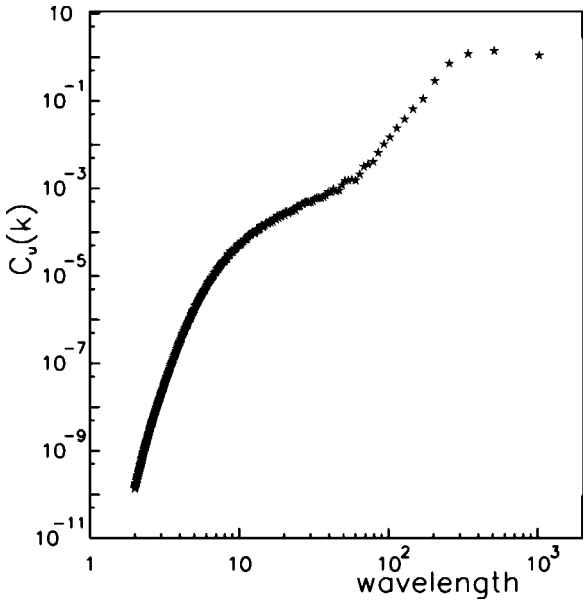

FIG. 4. Velocity structure factor $C_u(k)$ at time $t=15$ in the case with $\tau=10^{-4}, \beta=0.5$, and flux limiter scheme. $C_u(k)$ is in arbitrary units and the wavelength is measured in lattice spacings.

lengths and contributing little to the overall dynamics. A small bump can be seen at wavelength ~ 8 corresponding to capillary motion at interface length scale. A similar behavior was observed in binary fluids [59].

In the case with the upwind scheme the estimation of the growth exponent is more difficult since data are noisy and none of the R's shows a clear trend. From Fig. 5 it seems the system enters a late regime characterized by an exponent consistent with the value $1/2$. We believe that this behavior is due to spurious terms in the macroscopic equations that

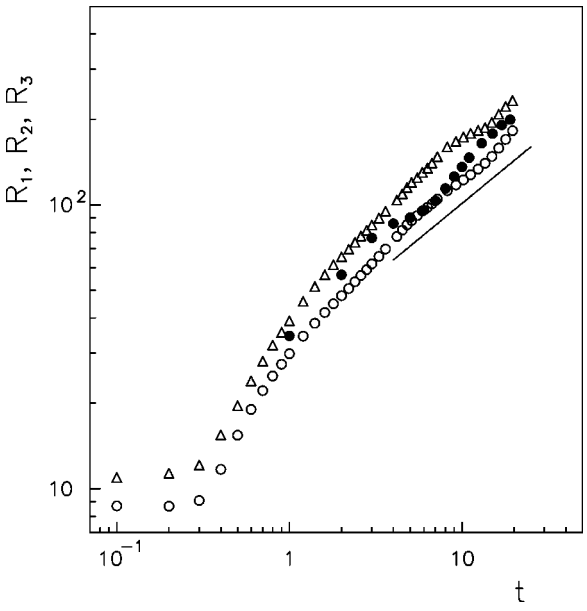

FIG. 5. Evolution of domains size in the case with $\tau=10^{-4}, \beta=0.5$ and the upwind scheme: $R_1(\Delta)$, $R_2(\circ)$, $R_3(\bullet)$. R's are measured in lattice spacings and R_1 as been rescaled by 4 000 000 to be shown in the same plot. The straight line has slope $1/2$.

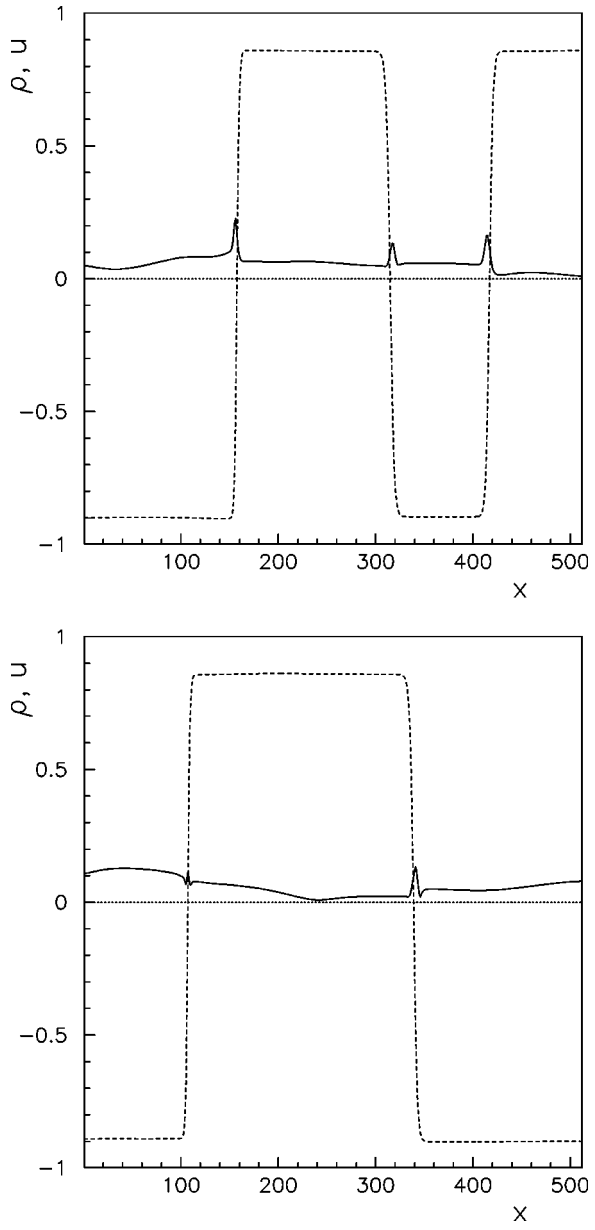

FIG. 6. Order parameter ρ (dashed line) and velocity modulus u (full line) profiles are shown along the line taken at $y=256$ lattice spacings from bottom at time $t=20$ for the upwind scheme (upper panel) and flux limiter scheme (lower panel) with $\tau=10^{-4}, \beta=0.5$.

are considerably larger when using the upwind scheme than in the case with flux limiter. These terms produce a numerical diffusivity when they are not negligible. This is confirmed by the analysis of the velocity fields in the two cases. In Fig. 6 we plot the order parameter ρ and velocity modulus u along a horizontal cross section of the system taken at the same long time. Two comments are in order here. It is quite unavoidable to have spurious velocities at interfaces where density gradients are present with LB models (irrespectively of the particular model used [60]). And also the present model shows this unpleasant feature. Nonetheless it is evident that the flux limiter scheme allows to dump considerably these spurious contributions. Indeed, with flux limiter the maximum value of velocity at interface is 0.13 (Ma

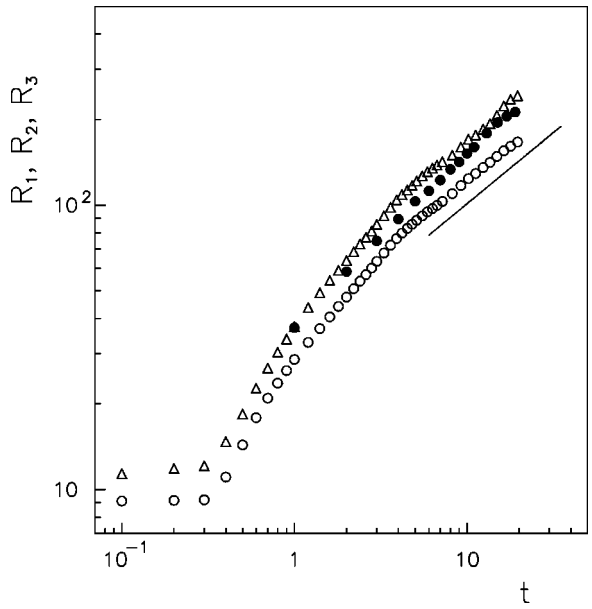

FIG. 7. Evolution of domains size in the case with $\tau=10^{-3}, \beta=0.5$, and flux limiter scheme: $R_1(\Delta)$, $R_2(\circ)$, $R_3(\bullet)$. R's are measured in lattice spacings and R_1 as been multiplied by 4 000 000 to be shown in the same plot. The straight line has slope $1/2$.

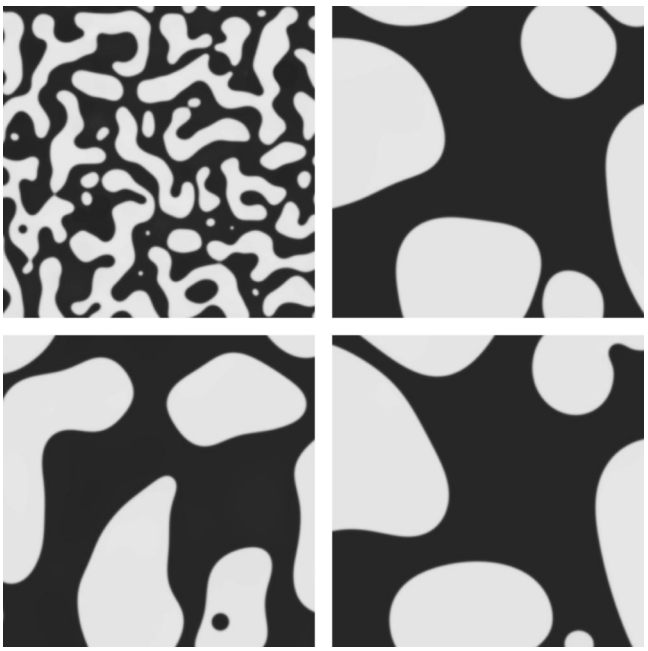

FIG. 8. Contour plots of a portion 512×512 of the whole lattice of the density n in the case with $\tau=10^{-3}, \beta=0.5$, and flux limiter scheme. Color code: black/white → liquid/vapor.

$=u/c_s=0.14$) while with the upwind it is about two times larger being 0.23 (Ma=0.26). The high value of the Mach number Ma makes the expansions (7) less reliable with the upwind scheme.

Due to the better performance of the flux limiter scheme we decided to adopt it for further simulations. In Fig. 7 we plot the three measures of domains size as function of time for the case $\tau=10^{-3}$ with symmetric composition. After initial growth all the quantities suggest the existence of the growth exponent $1/2$. This is in accordance with previous studies on liquid-vapor systems at high viscosity [41] at symmetric composition when growth is expected to be described by the Allen-Cahn theory of interfaces dynamics which gives an exponent $1/2$ [38] and hydrodynamics is not operating. Due to limits imposed by system size we cannot access very long times to probe whether the hydrodynamic regime is the late regime as previously argued [41]. Figure 8 shows density contour plots at consecutive times. Growth seems to be mainly driven by evaporation of vapor domains.

Finally, we considered the case of an off-symmetric system with a liquid fraction $\beta=0.45$. In Fig. 9 we plot the three measures of domains size as function of time for the case $\tau=10^{-4}$. After the initial growth all the quantities suggest the existence of a growth exponent $2/3$ which quite soon changes to $1/2$. In previous studies with a free-energy LB model it was found the growth exponent to be $2/3$ with liquid fraction $\beta=0.31$ [41] and $2/3$ crossing over to $1/2$ at $\beta=0.17$ [42]. The problem of off-symmetric liquid-vapor phase separation was recently addressed in Ref. [61]. There it was pointed out that in the case of a dispersion of liquid drops in vapor, the growth should proceed with an exponent $1/2$ and the result was proven in the case of highly asymmetric composition with $\beta=0.1$. We believe that we are probing a regime similar to that seen in two-dimensional binary fluids where, once hydrodynamics flow has made domains circular, Allen-Cahn growth takes over [36]. This interpretation seems to be confirmed by configurations of the system, presented in Fig. 10. They show that liquid drops in the vapor matrix are almost circular at $t=6$ so that the hydrodynamic mechanism is no more effective.

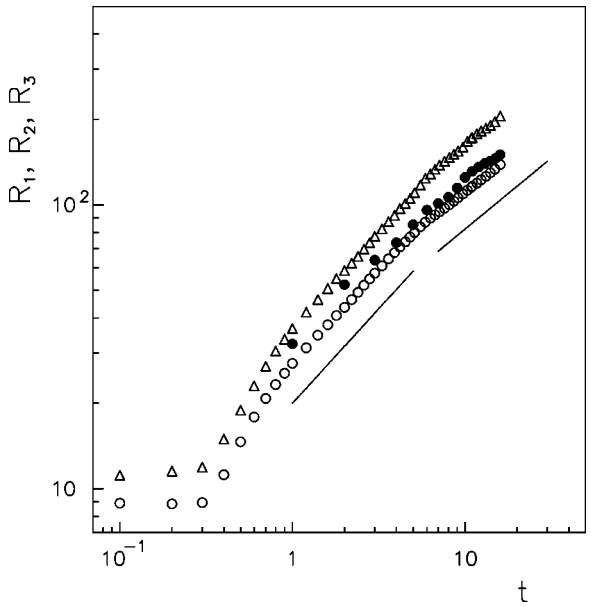

FIG. 9. Evolution of domains size in the case with $\tau=10^{-4}, \beta=0.45$, and flux limiter scheme: $R_1(\Delta)$, $R_2(\circ)$, $R_3(\bullet)$. R's are measured in lattice spacings and R_1 as been multiplied by 4 000 000 to be shown in the same plot. The straight lines have slopes $2/3$ and $1/2$.

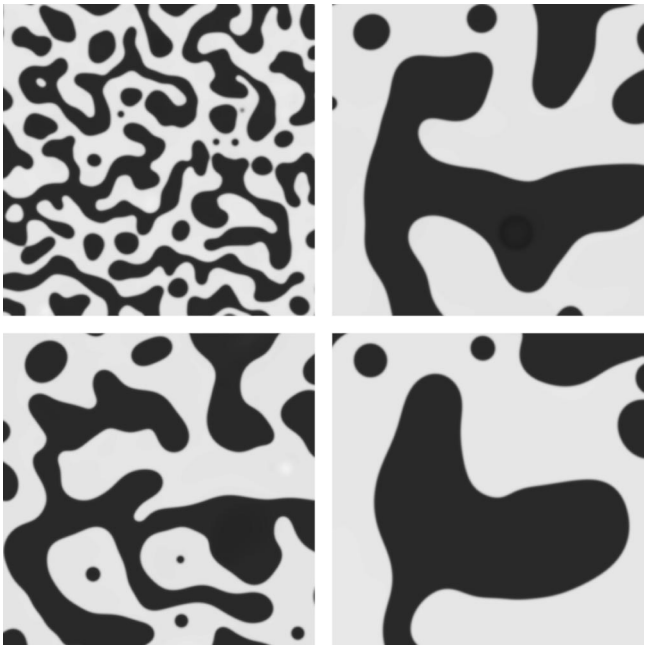

FIG. 10. Contour plots of a portion 512×512 of the whole lattice of the density n in the case with $\tau=10^{-4}, \beta=0.45$. Color code: black/white $\rightarrow$ liquid/vapor.

V. CONCLUSIONS

The correct choice of the numerical scheme is essential to recover the real physics of a fluid system subjected to LB simulations. In the case of a liquid-vapor system we have seen that simulation results exhibit significant changes when the numerical contribution of the finite difference scheme to the apparent value of the transport coefficients becomes comparable with the expected physical value. The numerical contribution of the first order upwind scheme is linearly dependent on the lattice spacing δs and switches to an higher order for the flux limiter scheme. Since $\delta s<1$, the flux limiter scheme reduces the computing effort in terms of required lattice nodes and gives physical results which are more accurate for the same number of lattice nodes per unit length. Spurious velocities at interfaces can be considerably damped and very low viscosity systems can be simulated preserving numerical stability. The main limitation comes from the requirement of a small time step when very low values of viscosity are needed. To give an idea of the CPU time we report that our code takes 6 h to perform 10^5 algorithm steps by using 32 xeon 3.055 GHz processors on the IBM Linux Cluster 1350 at CINECA [62] with Myrinet IPC network and the Portable Extensible Toolkit for Scientific Computation (PETSc 2.1.6) developed at Argonne National Laboratory, Argonne, Illinois [63].

The model allowed to clarify the picture of phase separation in liquid-vapor system. We found that the growth exponent depends on either the fluid viscosity and the system composition. When liquid and vapor are present in the same amount, the growth exponent is $2/3$ and $1/2$ at low and high viscosity, respectively. When the liquid fraction is less abundant than the vapor one, we can access a late time regime at low viscosity. In this regime the hydrodynamic transport is no more effective so we are able to see the crossover from the exponent $2/3$ to $1/2$ which is characteristic of the Allen-Cahn growth mechanism.

Finally, we note that our results as well as previous ones have been obtained in the case of isothermal systems. It would be interesting to incorporate the energy conservation equation into the model to allow nonuniform temperatures in the liquid-vapor system undergoing phase separation.

ACKNOWLEDGMENTS

V.S. acknowledges financial support from the University of Bari and thanks the IAC-CNR, Sezione di Bari, for hospitality. Computer runs were done on the parallel computing clusters at the Department of Physics, University of Bari and at the CINECA Consortium for Supercomputing (see Ref. [62]) in Casalecchio di Reno (Bologna) under an INFM grant. This work has been partially supported by MIUR (PRIN-2002).

[1] R. Benzi, S. Succi, and M. Vergassola, Phys. Rep. **222**, 145 (1992).
[2] D. H. Rothman and S. Zaleski, *Lattice Gas Cellular Automata: Simple Models of Complex Hydrodynamics* (Cambridge University Press, Cambridge, 1997).
[3] B. Chopard and M. Droz, *Cellular Automata Modeling of Physical Systems* (Cambridge University Press, Cambridge, 1998).
[4] D. A. Wolf-Gladrow, *Lattice Gas Cellular Automata and Lattice Boltzmann Models* (Springer Verlag, Berlin, 2000).
[5] S. Succi, *The Lattice Boltzmann Equation for Fluid Dynamics and Beyond* (Clarendon Press, Oxford, 2001).
[6] H. Grad, Commun. Pure Appl. Math. **2**, 331 (1949).
[7] S. Chapman and T. G. Cowling, *The Mathematical Theory of Non-Uniform Gases*, 2nd ed. (Cambridge University Press, Cambridge, 1961).
[8] W. G. Vincenti and C. H. Kruger, *Introduction to Physical Gas Dynamics* (Wiley, New York, 1965).
[9] J. M. Burgers, *Flow Equations for Composite Gases* (Academic Press, New York, 1969).
[10] K. Huang, *Statistical Mechanics*, 2nd ed. (Wiley, New York, 1987).
[11] T. I. Gombosi, *Gaskinetic Theory* (Cambridge University Press, Cambridge, 1994).
[12] V. Sofonea and R. F. Sekerka, Physica A **299**, 494 (2001).
[13] X. Shan and H. Chen, Phys. Rev. E **47**, 1815 (1993).
[14] X. Shan and H. Chen, Phys. Rev. E **49**, 2941 (1994).
[15] F. J. Higuera, S. Succi, and R. Benzi, Europhys. Lett. **9**, 345 (1989).
[16] A. K. Gunstensen, D. H. Rothman, S. Zaleski, and G. Zanetti, Phys. Rev. A **43**, 4320 (1991).
[17] M. R. Swift, W. R. Osborn, and J. M. Yeomans, Phys. Rev.

Lett. **75**, 830 (1995).
[18] E. Orlandini, M. R. Swift, and J. M. Yeomans, Europhys. Lett. **32**, 463 (1995).
[19] M. R. Swift, E. Orlandini, W. R. Osborn, and J. M. Yeomans, Phys. Rev. E **54**, 5041 (1996).
[20] S. Chen and G. D. Doolen, Annu. Rev. Fluid Mech. **30**, 329 (1998).
[21] X. He, X. Shan, and G. D. Doolen, Phys. Rev. E **57**, R13 (1998).
[22] A. Lamura, G. Gonnella, and J. M. Yeomans, Europhys. Lett. **45**, 314 (1999).
[23] B. J. Palmer and D. R. Rector, Phys. Rev. E **61**, 5295 (2000).
[24] A. N. Kalarakis, V. N. Burganos, and A. C. Payatakes, Phys. Rev. E **65**, 056702 (2002).
[25] R. R. Nourgaliev, T. N. Dinh, T. G. Theofanous, and D. Joseph, Int. J. Multiphase Flow **29**, 117 (2003).
[26] X. He and L. S. Luo, Phys. Rev. E **56**, 6811 (1997).
[27] N. Cao, S. Chen, S. Jin, and D. Martinez, Phys. Rev. E **55**, R21 (1997).
[28] R. Mei and W. Shyy, J. Comput. Phys. **143**, 426 (1998).
[29] T. Seta, K. Kono, D. Martinez, and S. Chen, JSME Int. J., Ser. B **43**, 305 (2000).
[30] T. H. Lee and C. L. Lin, J. Comput. Phys. **171**, 336 (2001).
[31] V. Sofonea and R. F. Sekerka, J. Comput. Phys. **184**, 422 (2003).
[32] M. Watari and M. Tsutahara, Phys. Rev. E **67**, 036306 (2003).
[33] X. He, L. Luo, and M. Dembo, J. Comput. Phys. **129**, 357 (1996).
[34] X. He, Int. J. Mod. Phys. C **8**, 737 (1997).
[35] C. S. Sunder, G. Baskar, V. Babu, and D. Strenski, *Proceeding of the 10th International Conference on High Performance Computing, HiPC 2003*, Lecture Notes in Computer Science Vol. 2913 (Springer-Verlag, Berlin, 2003), p. 428.
[36] J. M. Yeomans, Annu. Rev. Comput. Phys. **VII**, 61 (2000).
[37] A. J. Bray, Adv. Phys. **43**, 357 (1994).
[38] S. M. Allen and J. W. Cahn, Acta Metall. **27**, 1085 (1979).
[39] R. Yamamoto and K. Nakanishi, Phys. Rev. B **49**, 14958 (1994).
[40] R. Yamamoto and K. Nakanishi, Mol. Simul. **16**, 119 (1996).
[41] W. R. Osborn, E. Orlandini, M. R. Swift, J. M. Yeomans, and J. R. Banavar, Phys. Rev. Lett. **75**, 4031 (1995).
[42] K. R. Mecke and V. Sofonea, Phys. Rev. E **56**, R3761 (1997).
[43] V. Sofonea and K. R. Mecke, Eur. Phys. J. B **8**, 99 (1999).
[44] R. J. LeVeque, *Numerical Methods for Conservation Laws* (Birkhäuser Verlag, Basel, 1992).
[45] E. F. Toro, *Riemann Solvers and Numerical Methods for Fluid Dynamics*, 2nd ed. (Springer-Verlag, Berlin, 1999).
[46] H. Chen, Phys. Rev. E **58**, 3955 (1998).
[47] R. Zhang, H. Chen, Y. H. Qian, and S. Chen, Phys. Rev. E **63**, 056705 (2001).
[48] L. S. Luo, Phys. Rev. Lett. **81**, 1618 (1998).
[49] L. S. Luo, Phys. Rev. E **62**, 4982 (2000).
[50] P. Bhatnagar, E. Gross, and M. Krook, Phys. Rev. **94**, 511 (1954).
[51] A. Cristea and V. Sofonea, Int. J. Mod. Phys. C **14**, 1251 (2003).
[52] Y. H. Qian, D. d'Humieres, and P. Lallemand, Europhys. Lett. **17**, 479 (1992).
[53] R. J. LeVeque, *Finite Volume Methods for Hyperbolic Problems* (Cambridge University Press, Cambridge, 2002).
[54] S. L. Teng, Y. Chen, and H. Ohashi, Int. J. Heat Fluid Flow **21**, 112 (2000).
[55] A. Cristea and V. Sofonea, Proceedings of the Romanian Academy Series A: Mathematics, Physics, Technical Sciences, Information Science 4, 59 (2003).
[56] A. Cristea and V. Sofonea, Cent. Eur. J. Phys. **2**, 382 (2004).
[57] V. Sofonea and R. F. Sekerka (unpublished).
[58] G. E. Karniadakis and A. Beskok, *Micro Flows: Fundamentals and Simulation* (Springer-Verlag, New York, 2002).
[59] V. M. Kendon, M. Cates, I. Paganobarraga, J. C. Desplat, and P. Bladon, J. Fluid Mech. **440**, 147 (2001).
[60] S. L. Hou, X. W. Shan, Q. S. Zou, G. D. Doolen, and W. E. Soll, J. Comput. Phys. **138**, 695 (1997).
[61] P. B. Warren, Phys. Rev. Lett. **87**, 225702 (2001).
[62] http://www.cineca.it.
[63] S. Balay, K. Buschelman, V. Eijkhout, W. Gropp, D. Kaushik, M. Knepley, L. C. McInnes, B. Smith, and H. Zhang, Tech. Rep. ANL-95/11 - Revision 2.1.6, Argonne National Laboratory, http://www.mcs.anl.gov/petsc (2003).